Coherent twin-oriented Al_3Sc-based precipitates in Al matrix

Sankaran Shanmugam,[1] Martin Peterlechner,[2] Mohamad Riza Iskandar,[3] Ujjal Saikia,[4] Vladislav Kulitckii,[2] Marta Lipińska-Chwałek,[5] Joachim Mayer,[3,5] Harald Rösner,[2] Tilmann Hickel,[4,6] Sergiy V. Divinski,[2,*] and Gerhard Wilde[2]

[1] *Department of Metallurgical and Materials Engineering, Indian Institute of Technology Madras, Chennai-600036, India*

[2] *University of Münster, Institute of Materials Physics, Wilhelm-Klemm-Str. 10, 48149 Münster, Germany*

[3] *Central Facility for Electron Microscopy, RWTH Aachen University, 52074 Aachen, Germany*

[4] *Department of Computational Materials Design, Max-Planck-Institut für Eisenforschung GmbH, Max-Planck-Straße 1, 40237 Düsseldorf, Germany*

[5] *Ernst Ruska-Centre for Microscopy and Spectroscopy with Electrons, Forschungszentrum Jülich, 52425 Jülich, Germany*

[6] *BAM Bundesanstalt für Materialforschung und -prüfung, Richard-Willstätter-Str. 11, 12489 Berlin, Germany*

(Dated: December 6, 2022)

Al_3(Sc,Zr,Ti) nanoparticles with an ideal twin-type orientation relationship to Al host matrix were found in cold-rolled and subsequently annealed Al-based alloy. Atomic-scale investigations using high-resolution scanning transmission electron microscopy identified particles that form prominent coherent (111) twin-type interfaces along their longer facets and semi-coherent twin interfaces on their shorter facets. Ab-initio calculations showed that a coherent Al/Al_3Sc twin-like phase boundary corresponds to a local energy minimum. A model is proposed explaining the formation of the twin orientation relationship of an Al_3Sc nanoparticle with the Al host matrix.

Keywords: Al-based alloy; precipitation; twin orientation relationship

Incorporation of coherent and ordered nano-sized precipitations distributed randomly in a crystalline bulk is considered as an attractive concept for tremendous strength enhancement[1], simultaneous improvement of functional properties of advanced materials[2], and even to overcome the trade-off between strength and plasticity[3,4]. Typically, the precipitates with a relatively small lattice mismatch to the matrix are reported as coherent, semi-coherent or incoherent[5], and, predominantly, they feature a cube-on-cube orientation relationship (OR) for a broad class of materials. Very recently, a new type of ordered precipitates, the T-precipitates, was discovered in γ-γ' Ni-based superalloys exhibiting an OR that is close to twin-matrix OR[6,7].

Formation of lath-shaped Ag precipitates with an OR close to twin-matrix OR has been reported for a FCC Cu-6at.%Ag alloy[8]. The twin plane was inclined to the habit plane by 15.8° and the (111) planes of Cu and Ag were misoriented by about 2° due to the relatively large lattice mismatch of the two lattices[8]. However, in all reported cases, the T-precipitates revealed significant deviations with respect to the ideal twin-type orientation relationship. Moreover, the appearance of twin boundaries in materials with a low (the Cu-6at.%Ag alloy) or medium (Ni-based superalloys) stacking fault energy is not unexpected, but such T-precipitates (or twin-type phase boundaries) were never reported for Al-based alloys, although coherent T-type precipitates would provide even a higher potential for material's strengthening, featuring an enhanced resistance with respect to dislocation motion.

The Al-based alloys are in the focus of intensive research owing to their exceptional mechanical properties and microstructure stability at high temperatures[9]. Significant attention was paid to the production of non-heat treatable high-strength Al alloys with minor additions of Sc and Zr along with other elements[10]. Both, Sc and Zr, form $L1_2$-ordered Al_3Sc and Al_3Zr phases. At ambient conditions, the equilibrium lattice parameter of Al_3Sc (about 4.103 Å[11]) is slightly larger than that of pure Al (4.05 Å[12]), the critical size for the coherency loss was observed to be in the range of 20–40 nm[13,14] and similar values have been obtained by DFT-calculations[15]. Zirconium substitution decreases the lattice parameter of Al_3(Sc,Zr) precipitates, resulting in a decrease of the lattice parameter misfit with the Al matrix.

Marquis and Seidman[16] substantiated that the equilibrium shape of the Al_3Sc precipitates in the cast material with 0.3% Sc at 300°C is a great rhombicuboctahedron. However, a cube-shape morphology of the Al_3(Sc, Zr) precipitates with cube-on-cube OR in the as-cast state was frequently reported[17–21].

In the current study, we report on detailed high resolution scanning transmission electron microscopy (HR-STEM) of Al_3(Sc, Zr, Ti) $L1_2$-ordered precipitates in a severely cold-rolled (cross-directional rolling up to 95%) and subsequently annealed Al-Sc-Zr-Ti alloy. For the first time, ideal T-type Al_3Sc-based precipitates, i.e. with a coherent twin OR to the host Al matrix, are reported. The experimental observations are compared with DFT-informed calculations for its energy and chemistry.

Since the stacking fault energy in Al is relatively high, T-precipitation seems not so likely to happen. However, this new fundamental observation proves the existence of T-precipitates. Thus, it also calls for a theoretical investigation with respect to the nature, origin, interface properties, coherency issues, etc. to understand their formation.

Experimental and theoretical details. The material used in the study was an AA5024 commercial alloy with the following chemical composition: Al-4.57Mg-0.2Sc-0.09Zr-0.35Mn-0.14Fe-0.09Si (in wt.%). It was processed via hot-extrusion after casting. A detailed investigation of the initial microstructure is reported in Refs. [22] and [23].

The material was subjected to severe plastic deformation via cross-directional cold-rolling up to 95% thickness reduction followed by annealing at 350°C for 100 h. TEM foils were prepared by mechanical grinding and subsequent electro-polishing at −20°C using a mixture of nitric acid and methanol in a 1:2 ratio at 10 V using Struers Tenupol-5. A TEM pre-examination was carried out with a FEI Tecnai F20 operating at an accelerating voltage of 200 kV. Imaging and analytical TEM measurements were performed with a probe-corrected FEI Titan 80-200 ChemiSTEM microscope, equipped with a Super-X energy dispersive X-ray spectrometer. The high-resolution high-angle annular dark-field scanning transmission electron microscopy (HAADF-STEM) images were Noise-filtered using the ERC NLfilter by Du[24], and subsequently Wiener-filtered.

First principles total energy calculations were performed with density functional theory (DFT)[25] as implemented in the Vienna Ab-initio Simulation Package (VASP)[26]. We used projector-augmented wave (PAW) potentials[27] with the generalised gradient approximation Perdew-Burke-Ernzerhof (PBE)[28]. Phase boundary (PB) and twin boundary (TB) interfaces were modelled with periodically repeated orthorhombic cells using a super-cell approach. We used a kinetic energy cutoff of 425 eV for plane waves with a k-mesh equivalent to a k-mesh of 22×22×22 bulk Al, which ensure convergence of interface energies within 1 meV/Å^2.

Results. After the annealing at 350°C, a large density of nano-scale Al_3Sc-based precipitates

has been observed. Dominantly, these (nearly spherical) precipitates with typical sizes in the range of 10–30 nm were found to be coherent with the matrix, featuring the expected cube-on-cube OR. However, a detailed inspection also revealed the existence of larger (20 to 40 nm-sized) faceted Al_3Sc-based precipitates with a different OR to the matrix.

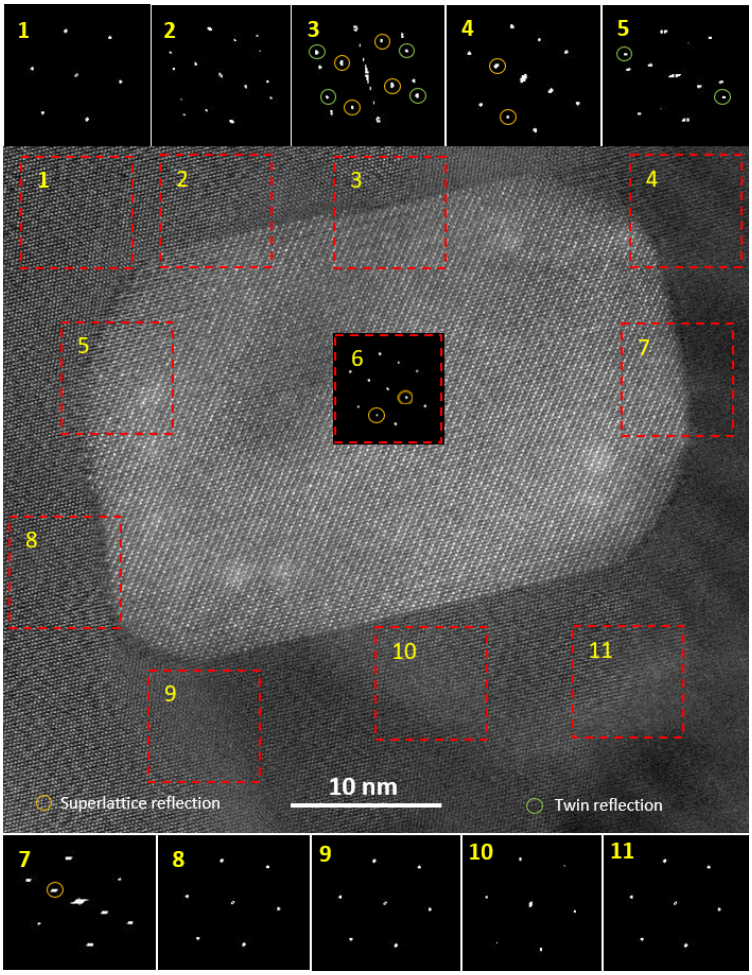

FIG. 1. High-resolution HAADF-STEM image of the $Al_3(Sc,Zr,Ti)$ precipitate revealing a special orientation with the Al matrix. The red square boxes (numbered 1 to 11) represent FFTs for the selected regions which confirm the common [110] zone axis for the matrix and the precipitate. The double diffraction-spots (exemplary shown by green circles on FFTs 3 and 5) indicate twin-boundary relation. On the FFTs recorded for the precipitate, the superlattice-spots (yellow circles on FFTs 3, 4, 6, and 7) prove the $L1_2$ order of the $Al_3(Sc,Zr,Ti)$ phase.

Figure 1 shows a high-resolution HAADF-STEM image of a faceted $Al_3(Sc, Zr, Ti)$ precipitate. The precipitate has coarsened to a dimension of about 37×25 nm^2 (in projection) during the long annealing treatment and displays clear facets. Fast-Fourier-Transforms

(FFTs) numbered 1 to 11 are obtained from the corresponding regions indicated by red square boxes, Fig. 1, confirming the [110] zone axis as imaging condition for both matrix and precipitate. The particle does not display Moiré fringes since it is not covered by the matrix (excavated). The prominent traces of (111) planes in the particle and surrounding matrix are clearly misoriented substantiating the absence of a cube-on-cube OR in this case.

The FFTs numbered 2, 3, 5, and 7 contain diffraction spots (exemplary shown by green circles) typical for twin boundaries. Furthermore, superlattice reflections (yellow circles) confirm clearly the ordered $L1_2$ structure of Al_3(Sc, Zr, Ti), Fig. 1.

The FFT analysis of the Al matrix around the entire precipitate, Fig. 1, inserts 1–5, 7–11, reveals the same orientation without any notable rigid-body rotation. The particle lattice, distinguished by the super-structure reflections, clearly reveals a novelty of the present paper, namely a coherent twin OR with the Al matrix,

$$(111)_{\mathrm{Al}} \parallel (111)_{\mathrm{Al_3Sc}} \quad \text{and} \quad [11\bar{2}]_{\mathrm{Al}} \parallel [11\bar{2}]_{\mathrm{Al_3Sc}} \tag{1}$$

An enlarged HAADF-STEM image in Fig. 2(a) shows the interface between the T-type Al_3(Sc,Zr) precipitate and the Al matrix at the edge of the longer interface in Fig. 1 in more detail revealing atomically sharp {111} facets. The long $(1\bar{1}1)$ facet of the particle displays a further novelty; that is a 'coherent twin-like phase (particle/matrix) interface'. The FFTs in Figs. 2 (b) and (c) are deduced for the Al matrix (green square in (a)) and the Al_3(Sc, Zr) precipitate (red square in (a)), respectively. The twin system is identified as $(1\bar{1}1)\langle\bar{1}12\rangle$ with an angle between the twinned (111) planes of $(109.3 \pm 0.3)^\circ$. The angle between Al (111) planes and the twin interface is $(54.7 \pm 0.3)^\circ$, as illustrated in the supplementary (Fig. S3).

The shorter particle-matrix interfaces correspond to incoherent twin-type phase boundaries. Misfit dislocations are found at the facet-corners, as shown in an exemplary analysis in Fig. 2(a) (see Burgers' circuits). For the (020) facet of the particle we find that the closing failure lies in the $(1\bar{1}1)$ plane along the $[\bar{1}12]$ direction and has a magnitude of $\frac{a}{4}[\bar{1}12]$. Two possible explanations can be provided for this observation. First, this is a misfit (edge) dislocation with the indicated Burgers vector lying parallel to a particular (111) nano-facet along the (112) direction which is generally sessile in nature. Alternatively, one can also think about a projection of a full $\frac{a}{2}[110]$ dislocation with the edge component of $\frac{a}{4}[\bar{1}12]$. This would correspond to a misfit dislocation (which is glissile in nature) having a mixed charac-

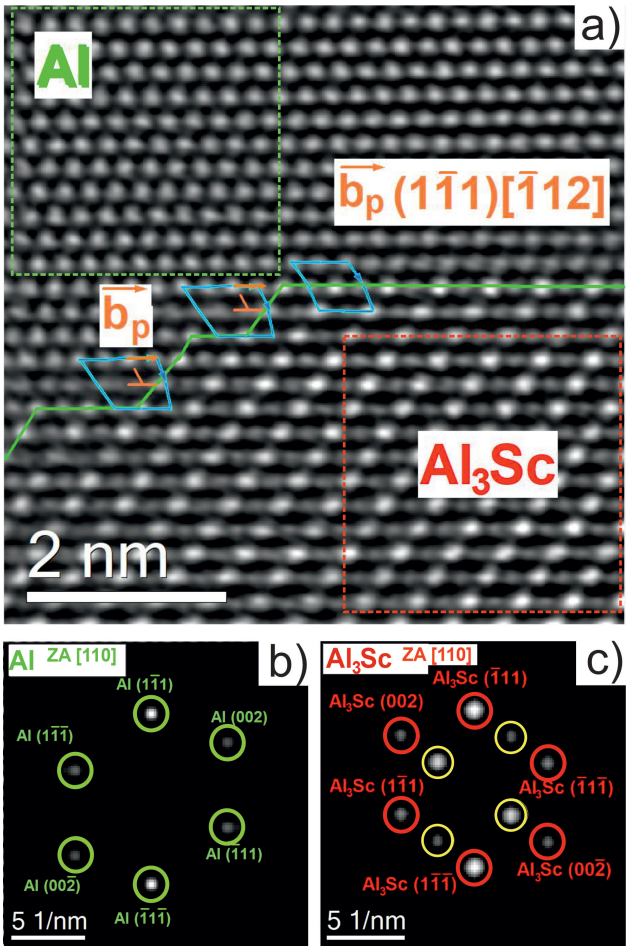

FIG. 2. (a) Atomic resolution HAADF-STEM image of an $Al_3(Sc, Zr)$ precipitate – Al matrix interface, displaying atomically sharp facets (filtered). The facet-corner features dislocations (see two Burgers' circuits) with insertion of additional Al planes. (b, c) The FFTs from the Al matrix (green box in (a)) and the $Al_3(Sc, Zr)$ precipitate (red box in (a)), respectively. The twin system is identified as $(1\bar{1}1)\langle\bar{1}12\rangle$ and the $(1\bar{1}\bar{1})$ planes are inclined to the twin particle/matrix interface at $(54.7 \pm 0.3)°$. In (c), the superlattice reflexes are encircled in yellow.

ter described by its inclination to projection direction, which is in our case 60°. In fact, the $\frac{a}{4}\langle 112\rangle$ closing failures were observed as the edge components of 60° $\frac{a}{2}\langle 110\rangle$ dislocations[29]. A detailed analysis is provided in the supplementary material.

Shockley partials of the type $\frac{a}{6}\langle 112\rangle$ terminating at the interface are completely ruled out for two reasons: (i) the magnitude of the observed projected Burgers vector is larger than the full magnitude of the Shockley partial, and (ii) the stacking fault associated with the partial should be observable in the HR-TEM micrograph. A high-resolution image of

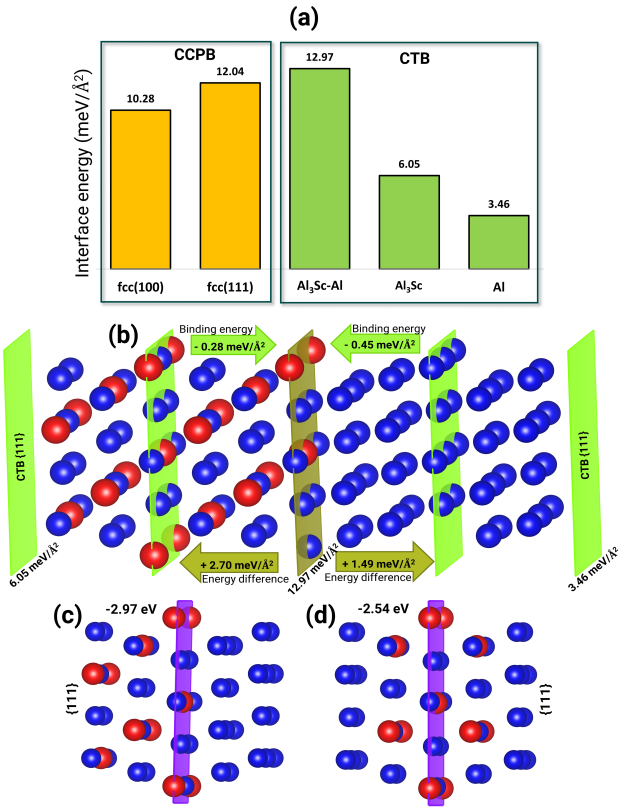

FIG. 3. (a) DFT calculated energies of cube-on-cube phase (CCPB) and coherent twin (CTB) boundaries. (b) Energetic of three different scenarios: twin boundary between Al_3Sc and Al matrix, within Al_3Sc matrix and within Al matrix. For the last two scenarios, moving twin boundary to either side will leave a fcc (111) phase boundary between Al_3Sc and Al. (c) Segregation of six Sc atoms to one side and (d) both sides of the twin interface.

an interface and corner indicating additional planes is shown in Fig. S5 (see Supplementary Material).

A Geometrical Phase Analysis[30] was carried out using the HAADF STEM image of a small Al_3Sc particle in order to estimate the misfit strain inside the precipitate and at the particle-matrix interfaces (see Figs. S3, S5–S7). The results show that the relative misfit strain is about 0.8%, which is in the range of the noise level.

To explain the observation, we note that severe cold rolling of the Al-Sc-Zr-Ti alloy produces a high density of nano-twins, stacking faults and dislocations. This is related to the reduction of the stacking fault energy of Al by the additions of Sc and Zr, as predicted by DFT calculations[31,32].

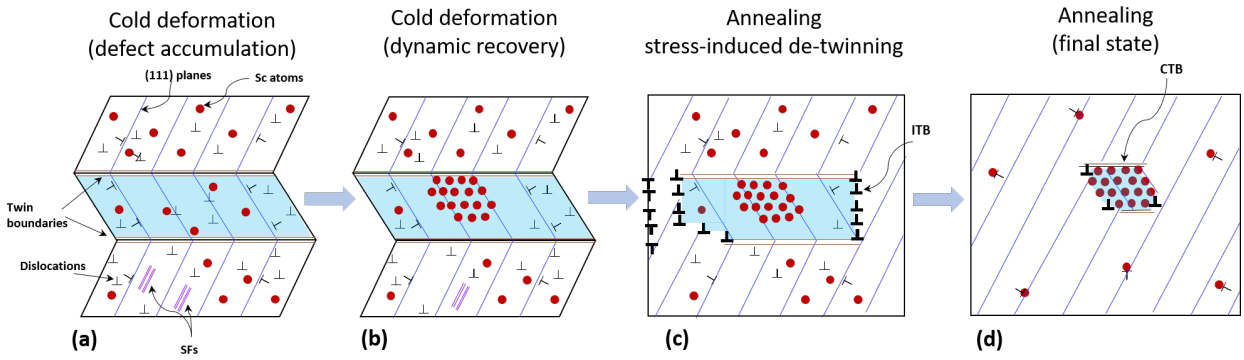

FIG. 4. Schematics of the coherent-twin particle growth: (a) a high density of dislocations, nano-twin lamella (highlighted by cyan color) with coherent twin boundaries (CTBs), stacking faults (SFs) and other defects due to cross-rolling at room temperature. Contaminant shearing/crashing of existing Al_3Sc precipitates enhances the concentration of Sc atoms in the deformed Al matrix. (b) Enhanced (ballistic) diffusion of Sc atoms during deformation and dynamic recovery lead to a precipitation of Al_3Sc particles at a twin boundary inside of a twin lamella (with the cube-on-cube OR with the local Al matrix). (c) Recovery of dislocations, stacking faults, and twins upon annealing; some of these defects are pinned by Sc atoms and by the Al_3Sc precipitates; nucleation and propagation of twin dislocations (thick symbols) and resulting motion of ITBs due to residual stresses; (d) Resulting Al_3Sc precipitates with a twin OR to the matrix; remnant CTBs as phase boundaries at the (111) facets of precipitates and remnant ITBs as phase boundaries at others, non-(111) facets.

Our DFT results reveal that the energy for a coherent twin interface between Al_3Sc and the Al matrix is only slightly larger than the energies of both, the (100) and (111) phase boundaries of a coherent cube-on-cube Al_3Sc precipitate (Fig. 3(a)). The twin boundary energies for both phases (Al_3Sc or Al) are smaller than that of the twin phase boundary, Fig. 3(a). Given their presence due to the cold rolling, however, it seems to be evident that merging the precipitate interface and the twin boundary is energetically more favourable than their separation.

For a more detailed analysis, we, firstly, considered competing scenarios. As shown in Fig. 3(b), a precipitate interface three layers apart from the twin boundary already yields a binding energy of approx 0.5 meV/Å^2, which is 1.5 meV/Å^2 higher in energy as compared to the merged interface. At the same time this implies that twin boundaries are pinned to

the precipitate interface. On the other hand, a continuation of the growth of the precipitate such that it encloses the twin boundary, yields an energy increase of approx. 2.5 meV/Å^2. Hence, in both cases the sum of two interface energies is larger than that of the merged twin phase boundary.

Secondly, we have analysed the different segregation steps for a number of Sc atoms to different sites across coherent twin boundaries (CTBs) in Al (see Supplementary Material Fig. S9). Our initial choice of segregation sites for Sc was guided by the experimentally predicted arrangement of Sc atoms in Al_3Sc/Al twin interface as shown in Fig. 2(b). The segregation of Sc atoms from the Al bulk matrix to the CTB is favourable with a tendency to precipitate along the Al (111) plane. For two Sc atoms, segregation to the twin interface plane is the most favourable scenario. Once the CTB plane is covered by Sc atoms, the next Sc atoms prefer to segregate to the second-next plane from the CTB. Here, we consider two different segregation configurations for six Sc atoms as shown in Fig. 3(c) and (d). In the first configuration, six Sc atoms segregated to the same side of the CTB which is energetically more favourable (with an energy difference of 0.43 eV) than the second configuration where Sc atoms segregated to both sides of the twin interface. This confirms that already upon the nucleation of the precipitate, the twinned interface is the preferred configuration.

Based on the experimental data and the DFT-informed analysis, we assume that the overall formation of T-particles proceeds as shown schematically in Fig. 4. We focus the description to the formation of purely T-type Al_3Sc particles and neglect the nucleation. The Zr and Ti atoms play most likely a minor role and they are not considered presently.

In our model, we assume that severe plastic deformation leads to a high density of defects, including twin lamellae with coherent twin boundaries, and a re-distribution of Sc atoms in the matrix, Fig. 4(a). The onset of defect rearrangements and Sc segregation takes place during the dynamic recovery stage before deformation ceases. The DFT calculations predict that individual Sc atoms can segregate at CTBs, and a larger number of Sc atoms co-segregate at one side of a CTB (forming a nucleus of an Al_3Sc precipitate at one side of the CTB with the typical cube-on-cube OR with the local Al matrix), Fig. 4(b). The lower interface excess energy of this configuration (i.e. sharing one interface with the CTB) reduces the work of nucleation of the Al_3Sc precipitates, thus favoring their formation. At the same time, this configuration stabilizes the interface between matrix and precipitate that shows a twin orientation relationship. Alternatively, an Al_3Sc precipitate might nucleate somewhere

inside of a twin lamella.

Upon heating, further recovery proceeds via defect and grain boundary rearrangements. Twinning dislocations (thick symbols in Fig. 4) nucleate at twin lamellae[33] and move under residual stresses. In this way de-twinning is initiated in which incoherent twin boundaries (ITBs) are formed[33], Fig. 4(c) and subsequently deformation-induced dislocations as well as stacking-faults are annihilated, except some defects pinned by impurities. It has recently be shown that the kinetic energy barrier for stacking fault recovery is reduced by Zr, enhancing this de-twinning process[34]. The twinning dislocations and ITBs are successively getting pinned by the Al_3Sc precipitate, giving rise to the formation of both coherent and 'non-coherent-(111)' facets, Fig. 4(d). The DFT calculations have also shown that the propagation of a twinning dislocation through the Al_3Sc particle will increase the system energy, since two boundaries (precipitate/matrix (111) interface and a twin boundary inside the Al_3Sc particle) have to be created. As a result of the de-twinning process, the twinning dislocations are therefore stopped at the side facets of the particle, Figs. 2(b) and 4(d).

Summary. The present atomically resolved STEM examination discovered novel T-type faceted Al_3(Sc,Zr,Ti) precipitates with an ideal twin OR with respect to the surrounding Al-matrix in severely deformed and annealed Al-Sc-Zr-Ti alloy. The longest facets of such precipitates correspond to (111) coherent twin (phase) boundaries.

The DFT calculations substantiate that the coherent Al/Al_3Sc twin interface corresponds to a local minimum of energy and there is an energy penalty for the twin boundary to 'escape' the particle; i.e. if the phase boundary moves away of the twin interface in any direction (towards the precipitate or Al matrix) the system energy is increasing. As an Al_3Sc-based particle nucleates inside of a nano-twin lamella, it has a common cube-on-cube orientation relation with the surrounding matrix inside of the lamella. Heat treatment prompts twin recovery, but motion of twin dislocations via ordered particle is hindered and the particle remains in the twin OR, Eq. (1), with the matrix featuring two opposite and almost coherent twin boundaries which are connected by (faceted) incoherent twin interfaces.

Prof. S. Sankaran thanks Alexander von Humboldt Foundation for his research stay in Germany through an AvH fellowship for experienced researchers. Financial support from the German Science Foundation (DFG) via research grants DI 1419/14-1 and HI 1300/13-1 is acknowledged. The DFG is further acknowledged for funding our TEM equipment via the Major Research Instrumentation Program under INST

211/719-1 FUGG.

---

* divin@uni-muenster.de

[1] J.Y. He, H. Wang, H.L. Huang, X.D. Xu, M.W. Chen, Y. Wu, X.J. Liu, T.G. Nieh, K. An, and Z.P. Lu. A precipitation-hardened high-entropy alloy with outstanding tensile properties. *Acta Materialia*, 102:187–196, 2016.

[2] L. Han, Z. Rao, Isnaldi R. Souza F., F. Maccari, Y. Wei, G. Wu, A. Ahmadian, X. Zhou, O. Gutfleisch, D. Ponge, D. Raabe, and Zh. Li. Ultrastrong and Ductile Soft Magnetic High-Entropy Alloys via Coherent Ordered Nanoprecipitates. *Advanced Materials*, 33(37):2102139, 2021.

[3] L. Liu, Y. Zhang, J. Han, X. Wang, W. Jiang, C.-T. Liu, Z. Zhang, and P.K. Liaw. Nanoprecipitate-strengthened high-entropy alloys. *Advanced Science*, 8(23):2100870, 2021.

[4] Y. Yang, T. Chen, L. Tan, J.D. Poplawsky, K. An, Y. Wang, G.D. Samolyuk, K. Littrell, A.R. Lupini, A. Borisevich, and E.P. George. Bifunctional nanoprecipitates strengthen and ductilize a medium-entropy alloy. *Nature*, 595:245–249, 2021.

[5] F.C Campbell. *Elements of metallurgy and engineering alloys*. ASM International, 2008.

[6] S. Vernier, J.-M. Franchet, C. Dumont, P. Vennégues, and N. Bozzolo. γ' precipitates with a twin orientation relationship to their hosting grain in a $\gamma - \gamma$' nickel-based superalloy. *Scripta Materialia*, 153:10–13, 2018.

[7] S. Vernier, JM. Franchet, C. Dumont, and N. Bozzolo. A Mechanism Leading to γ' Precipitates with 111 Facets and Unusual Orientation Relationships to the Matrix in $\gamma - \gamma$' Nickel-Based Superalloys. *Metall Mater Trans A*, 49:4308–4323, 2018.

[8] G. Rao, J.M. Howe, and P. Wynblatt. Analysis of the interfacial structure of a twinned variant of Ag precipitate in Cu–Ag alloys. *Scripta Metall. Mater.*, 30:731–736, 1994.

[9] J Royset and N Ryum. Scandium in aluminium alloys. *Int. Mater. Rew.*, 50(1):19–44, 2005.

[10] K.E. Knipling, R.A. Karnesky, C.P. Lee, D.C. Dunand, and D.N. Seidman. Precipitation evolution in Al-0.1Sc, Al-0.1Zr and Al-0.1Sc-0.1Zr (at.%) alloys during isochronal aging. *Acta Mater.*, 58:5184, 2010.

[11] Y. Harada and D.C. Dunand. Microstructure of Al_3Sc with ternary transition-metal additions. *Mater. Science Engineer. A*, 329–331:686–695, 2002.

[12] M. E. Straumanis and C. L. Woodward. Lattice parameters and thermal expansion coefficients of Al, Ag and Mo at low temperatures. Comparison with dilatometric data. *Acta Crystallographica Section A*, 27:549–551, 1971.

[13] S. Iwamura and Y. Miura. Loss in coherency and coarsening behavior of Al_3Sc precipitates. *Acta Mater.*, 52:591–600, 2004.

[14] S. Saha, T.Z. Todorova, and J.W. Zwanziger. Temperature dependent lattice misfit and coherency of Al_3X (X = Sc, Zr, Ti and Nb) particles in an Al matrix. *Acta Mater.*, 89:109–115, 2015.

[15] A. Gupta, V. Kulitcki, B. Tas Kavakbasi, Yu. Buranova, J. Neugebauer, G. Wilde, T. Hickel, and S.V. Divinski. Precipitate-induced nonlinearities of diffusion along grain boundaries in Al-based alloys. *Physical Review Materials*, 2(7), JUL 9 2018.

[16] E.A. Marquis and D.N. Seidman. Nanoscale structural evolution of Al_3Sc precipitates in Al(Sc) alloys. *Acta mater.*, 49:1909, 2001.

[17] A.M. Samuel, S.A. Alkahtani, H.W. Doty, and F.H. Samuel. Role of Zr and Sc addition in controlling the microstructure and tensile properties of aluminum-copper based alloys. *Mater. and Design*, 88:1134, 2015.

[18] N.A. Belov, A.N. Alabin, and I.A. Matveeva. Optimization of phase composition of Al-Cu-Mn-Zr-Sc alloys for rolled products without requirement for solution treatment and quenching. *J. Alloys and Comp.*, 583:206, 2014.

[19] B. Liu, J. Tao, S. Li, and M. Li. Evolution of Microstructure and Precipitates with Cycle Annealing Temperature of an Al-6Mg-Mn-Sc-Zr Alloy. *Mater. and Manuf. Proc.*, 22:1, 2007.

[20] J.H. Li, M. Wiessner, M. Albu, S. Wurster, B. Sartory, F. Hofer, and P. Schumacher. Correlative characterization of primary Al_3(Sc,Zr) phase in an Al-Zn-Mg based alloy. *Mater. Charact.*, 102:62, 2015.

[21] Y. Zhao, W. Zhang, B. Koe, W. Du, W. Wang, M. Wang, E. Boller, A. Rack, Z. Sun, D. Shu, B. Sun, and J. Mi. Multiscale characterization of the nucleation and 3D structure of Al3Sc phases using electron microscopy and synchrotron X-ray tomography. *Mater. Charact.*, 164:110353, 2020.

[22] A. Mogucheva, E. Babich, B. Ovsyannikov, and R. Kaibyshev. Microstructural evolution in a 5024 aluminum alloy processed by ECAP with and without back pressure. *Mater. Science Engineer. A*, 560:178–192, 2013.

[23] Yu. Buranova, V. Kulitskiy, M. Peterlechner, A. Mogucheva, R. Kaibyshev, S. V. Divinski, and G. Wilde. Al_3(Sc,Zr)-based precipitates in Al-Mg alloy: Effect of severe deformation. *Acta Materialia*, 124:210–224, FEB 1 2017.

[24] H. Du. A nonlinear filtering algorithm for denoising HR(S)TEM micrographs. *Ultramicroscopy*, 151:62–67, 2015.

[25] P. Hohenberg and W. Kohn. Inhomogeneous electron gas. *Physical Review*, 136(3B):B864, 1964.

[26] G Kresse and J Furthmüller. Efficient iterative schemes for ab initio total-energy calculations using a plane-wave basis set. *Physical Review B*, 54:11169, 1996.

[27] J.P Perdew and Y. Wang. Accurate and simple analytic representation of the electron-gas correlation energy. *Physical Review B*, 45(23):13244, 1992.

[28] J.P Perdew, K. Burke, and M. Ernzerhof. Generalized gradient approximation made simple. *Physical review letters*, 77(18):3865, 1996.

[29] Michael J. Mills and Pierre Stadelmann. A study of the structure of Lomer and 60° dislocations in aluminium using high-resolution transmission electron microscopy. *Philosophical Magazine A*, 60(3):355–384, 1989.

[30] M. Hÿtch, E. Snoeck, and R. Kilaas. Quantitative measurement of displacement and strain fields from HREM micrographs. *Ultramicroscopy*, 74:131–146, 1998.

[31] X. Zhang, X. Ren, H. Li, Y. Zhao, Y. Huang, Y. Liu, and Z. Xiao. Interfacial properties and fracture behavior of the $L1_2$-Al_3Sc//Al interface: Insights from a first-principles study. *Appl. Surf. Sci.*, 515:146017, 2020.

[32] Q. Gao, H. Zhang, R. Yang, Z. Fan, Y. Liu, J. Wang, X. Geng, Y. Gao, S. Shang, Y. Du, and Z. Liu. Effect of alloying elements on the stacking fault energies of dilute Al-based alloys. *J. Min. Metall. Sect. B-Metall.*, 54:185–196, 2018.

[33] J. Wang, N. Li, O. Anderoglu, X. Zhang, A. Misra, J.Y. Huang, and J.P. Hirth. Detwinning mechanisms for growth twins in face-centered cubic metals. *Acta Materialia*, 58:2262–2270, 2010.

[34] G.Y. Li, Y.Q. Wang, J.D. Zuo, M. Zhang, C. He, X. Feng, Y. Luan, J.H. andd Lu, J.Y. Zhang, S. Cazottes, D. Kiener, G. Liu, and J. Sun. Zr addition-dependent twin morphology evolution and strengthening response in nanostructured Al thin films. *Materialia*, 16:101076, 2021.